AJNR

Computed Tomography of Temporal Bone Pneumatization: 1. Normal Pattern and Morphology

Chat Virapongse, Mohammad Sarwar, Sultan Bhimani, Clarence Sasaki and Robert Shapiro

AJNR Am J Neuroradiol 1985, 6 (4) 551-559
http://www.ajnr.org/content/6/4/551

Computed Tomography of Temporal Bone Pneumatization: 1. Normal Pattern and Morphology

Chat Virapongse[1, 2]
Mohammad Sarwar[1]
Sultan Bhimani[1]
Clarence Sasaki[3]
Robert Shapiro[4]

The pneumatization of 141 "normal" temporal bones on computed tomography (CT) was evaluated in 100 patients (age range, 6–85 years). Because of the controversy surrounding the sclerotic squamomastoid (mastoid), temporal bones with this finding were discarded. A CT index of pneumatization was based on the pneumatized area and the number of cells seen within a representative scanning section. Results suggest that squamomastoid pneumatization follows the classic normal distribution and does not correlate with age, gender, or laterality. A high degree of symmetry was found in 41 patients who had both ears examined. In 35% of all temporal bones, the petrous apex was pneumatized, concordant with the findings of other investigators. Pneumatization extending into other regions of the temporal bone corresponded linearly with squamomastoid pneumatization. Air-cell configuration was variable. Air-cell size tended to increase progressively from the mastoid antrum. The scutum "pseudotumor" appearance caused by incomplete pneumatization was seen frequently, and should not be mistaken for mastoiditis or an osteoma. Thick sections producing partial-volume effect may also produce this spurious finding. Therefore, when searching for mucosal thickening due to mastoiditis, large air cells should preferably be analyzed.

Despite the inherent limitations, plain firm radiography has in the past played an important role in evaluating termporal bone pneumatization. Because high-resolution computed tomography (CT) is now the major imaging method for the ear, we attempted to define the normal CT morphology of temporal bone pneumatization and its pattern of distribution.

Anatomy of Temporal Bone Pneumatization

Developmental Anatomy

There is no agreement as to when pneumatization occurs. Some claim that pneumatized cells can be seen at 24 weeks of gestation [1–6], while others state that they are present at birth [7–10]. Microscopically, an air cell is lined by a single flat layer of epithelium separated from bone by subepithelial connective tissue. The epithelium and connective tissue constitute the mucous membrane of the air cell. According to Wittmaack [9], the activity of this subepithelial layer is largely responsible for air-cell formation. Radiographically (and macroscopically) air cells are not visible until after birth.

The development of air cells is preceded by the formation of bone cavities, a normal physiologic process related to periosteal activity [11, 12]. The bone cavities contain primitive bone marrow, which dedifferentiates into a loose mesenchymal connective tissue [6]. After the epithelial mucous membrane has invaginated, it in turn undergoes atrophy, leaving a thin residual lining membrane attached to the periosteum. "Recession" of the lining membrane and subepithelial bone resorption then further enlarge air cells [6, 11, 12], but apparently only in the presence of air [13].

This article appears in the July/August 1985 issue of *AJNR* and the September 1985 issue of *AJR*.

Received August 23, 1984; accepted after revision December 8, 1984.

Presented at the annual meeting of the American Society of Neuroradiology, Boston, June 1984.

[1] Department of Diagnostic Imaging, Section of Neuroradiology, Yale–New Haven Hospital, New Haven, CT 06510.

[2] Present address: Department of Radiology, Veterans Administration Hospital, 1601 Archer Rd., Gainesville, FL 32608. Address reprint requests to C. Virapongse.

[3] Department of Surgery, Section of Otolaryngology, Yale–New Haven Hospital, New Haven, CT 06510.

[4] Department of Radiology, Hospital of St. Raphael, New Haven, CT 06511.

***AJNR* 6:551–559, July/August 1985**
0195–6108/85/0604–0551

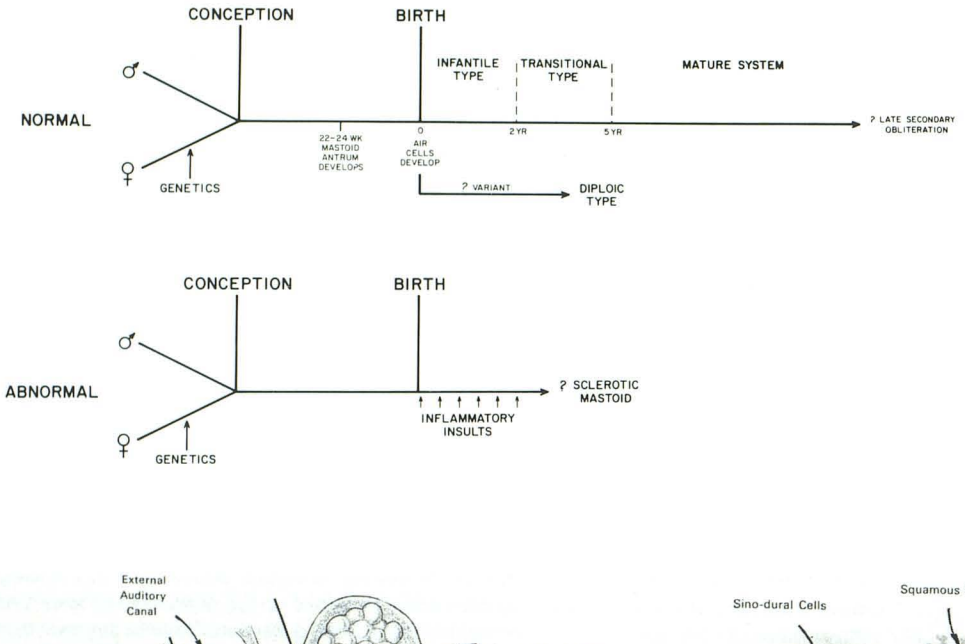

Fig. 1.—Normal development of air cells. Diploic system formerly considered to be similar to sclerotic system is now thought to be unrelated to inflammation, perhaps a genetic variant. Wittmaack's [9] views on sclerotic squamomastoid seem largely to be accepted.

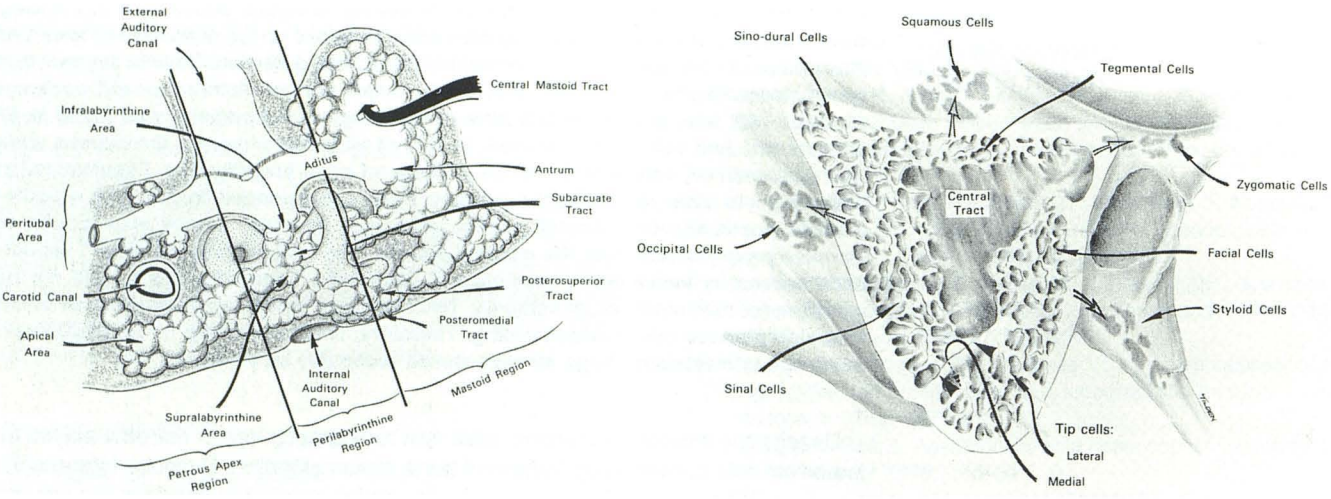

Fig. 2.—**A**, Drawing of left temporal bone in axial view showing distribution of regions, areas, and tracts of pneumatization according to classification of Allam [17]. **B**, Drawing of sagittal section of right squamomastoid demonstrating central tract and surrounding air cells. Note separation of tip cells into two groups by inferior petrosquamosal suture (*arrowheads*). *Open arrows* indicate extension of air cells into corresponding accessory region. (**A** and **B** reprinted from [19].)

The development of complete adult pneumatization can be divided into three stages: the infantile, from birth to 2 years of age; the transitional, from 2 to 5 years; and thereafter the adult [14, 15] (fig. 1). In the infantile stage, air cells begin to appear and are readily visible by 2 years. In the transitional stage, the squamomastoid undergoes gradual enlargement, with migration of air cells toward the periphery. Once the adult stage is attained, pneumatization ceases (fig. 1).

Adult Anatomy

The classification of temporal bone pneumatization is complex. Because there is no consensus [3, 16–20], Allam's [17] more simple classification will be described.

Pneumatization of the temporal bone may be divided into five regions, which in turn are subdivided into areas. The primary regions consist of the middle ear, squamomastoid (mastoid), perilabyrinthine, petrous apex, and accessory (fig. 2). (We prefer the term "squamomastoid" rather than "mastoid" to stress the dual origin of the mastoid [21].)

The squamomastoid consists of two key areas of pneumatization: the mastoid antrum (and central tract) and the peripheral area (figs. 3–5). The mastoid antrum lies superior. Inferiorly and laterally the antrum extends downward in the direction of the mastoid tip, forming an oblong space called the central tract (figs. 2B and 4A). On axial CT, the mastoid antrum lies at the level of the epitympanic recess (fig. 3D) and internal auditory canal (IAC). The central tract, a capacious space similar to the antrum, lies at a lower level corresponding to the external auditory canal (fig. 3C). Immediately surrounding the antrum are the periantral cells. The tegmental cells lie in the tegmen mastoideum above the mastoid antrum (fig.

Fig. 3.—Axial scans of left ear from inferior to superior. **A** and **B**, Inferior sections below external auditory canal. Infralabyrinthine cells are distributed posteromedial to carotid canal (CC). Air in eustachian tube (ET) is seen lateral to carotid canal. Some air cells extend into jugular spine (JS). Tip cells (T) are located in mastoid process subdivided by inferior septum (*curved arrows*). OM = occipitomastoid suture. **C**, At level of external auditory canal (E), central tract (C) is seen. Ventral are facial cells (F); dorsal are sinal cells (S). In this patient, large superior septum (*arrowhead*) is present. Note close relation between posteromedial tract (PM) and foveate impression (FI). I = internal auditory canal. **D**, At level of internal auditory canal (I), mastoid antrum (MA) is visible. Medially, posteromedial (PM) tract passes anteriorly below internal auditory canal (I). AP = air cell in petrous apex. **E** and **F**, Sections through epitympanic recess and mastoid antrum. Posteromedial to mastoid antrum (MA), sinodural cells (SD) are seen, laterally squamosal cells (SQ). Note "pseudotumor" (*arrow*). Medially, posterosuperior tract (PS) is present, passing medial to semicircular canals. Subarcuate tract (SA) passes below arch of superior semicircular canal (SS). Both supralabyrinthine tracts join to pneumatize petrous apex. Z = zygomatic accessory air cells; *arrowhead* = superior septum.

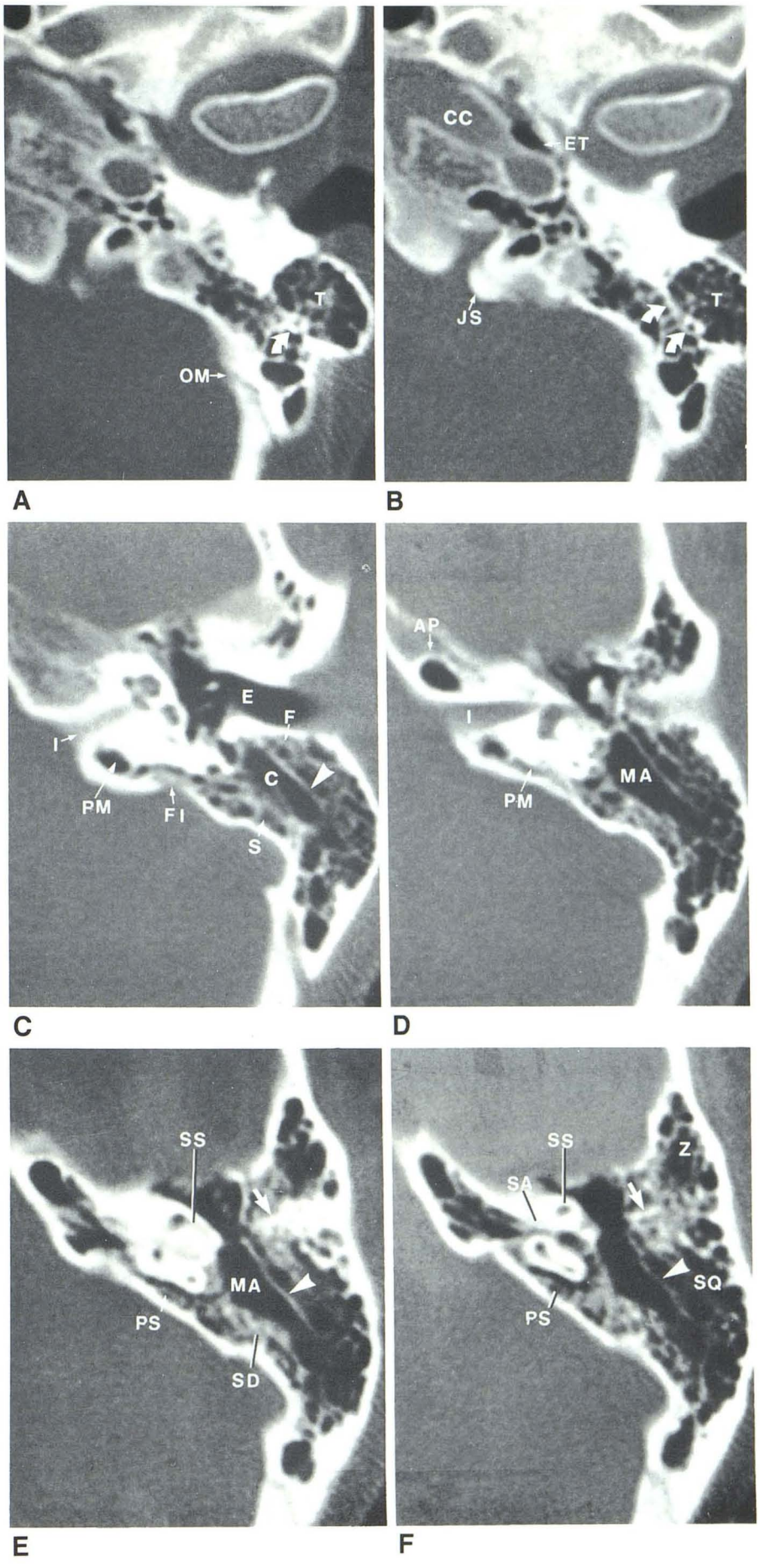

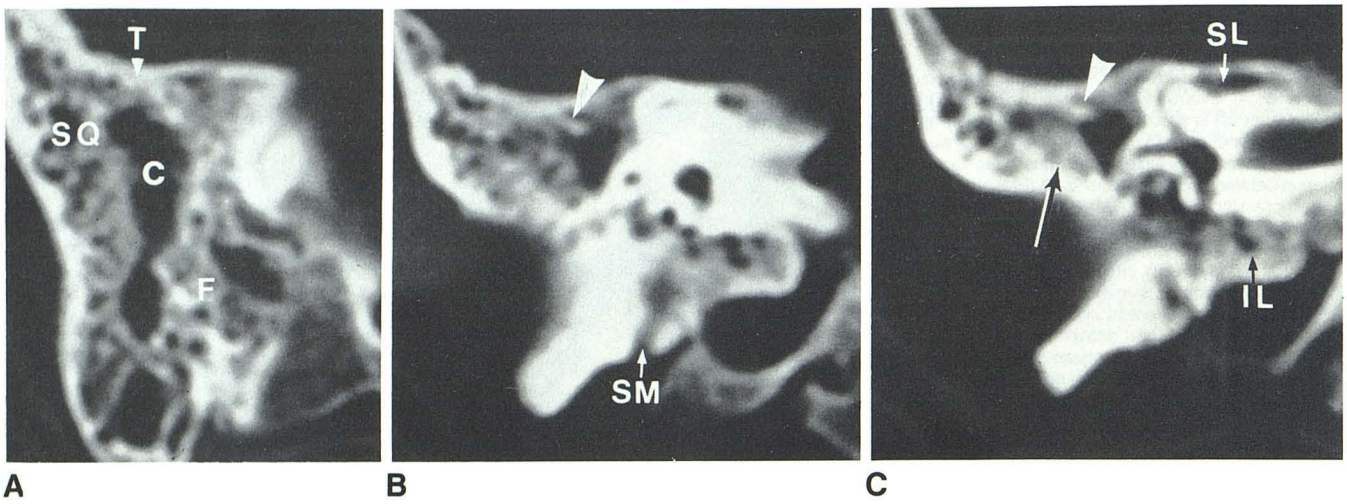

Fig. 4.—Coronal sections through right posterior temporal bone of dry skull from posterior to anterior. **A**, Section through central tract (C). F = facial cells; SQ = squamosal; T = tegmental cells. **B** and **C**, Sections through stylomastoid foramen (SM) demonstrating supra- (SL) and infralabyrinthine (IL) air cells. *Arrow* = scutum pseudotumor; *arrowhead* = superior septum projecting into mastoid antrum.

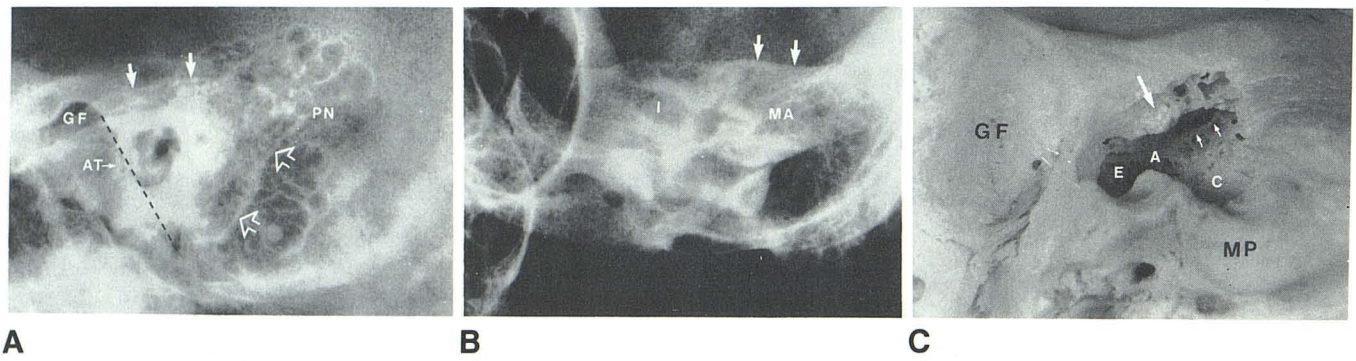

Fig. 5.—Law (**A**) and Stenvers (**B**) views of same ear showing extension of air cells beyond periantral triangle of Schillinger. Line drawn from glenoid fossa (GF) to parietal notch (PN) forms roof of triangle (*solid arrows*); line from parietal notch passing through sinus plate to terminate at lowest point of tympanomastoid suture represents posterior boundary (*open arrows*). Triangle is completed by ventral line (*dashed line*), which passes through anterior tympanic plate (AT). Note crisp, well defined margins of normal air cells. On Stenvers view (**B**), superior boundary is formed by tegmen (*arrows*). Note lateral columns of air cells extending from mastoid antrum (MA). I = internal auditory canal. **C**, Inferior view of same drilled-out dry skull to demonstrate epitympanic recess (E), aditus (A), and mastoid antrum. Central tract (C) is seen almost en face. Ridge of bone representing superior septum (*small arrows*) is observed from below in mastoid antrum; note size correlation with CT in fig. 4. Scutum is also drilled out to show incomplete pneumatization (i.e., scutum pseudotumor [*arrow*]) as seen in fig. 4. GF = glenoid fossa; MP = mastoid process.

4A) and are seen on higher axial cuts at the level of the topmost arch of the superior semicircular canal. The more posterior sinodural air cells are located in the posterosuperior angle of the pyramid, bounded by the dural plate above and the sinus plate below (fig. 3E). The sinal cells abutting the sinus plate lie at the level of the external auditory canal and mastoid process (fig. 3C). Lying ventrally, but separated from them by the central tract, are the facial cells (fig. 3C), adjacent to the vertical facial canal and posterior wall of the external ear canal. More inferiorly, below the central tract, are the tip cells, in the mastoid process and tip (figs. 3A and 3B).

The posterosuperior and posteromedial tracts pass medially from the antrum to pneumatize the medial pyramid (figs. 3D–3F). The posterosuperior tract is seen on "high" sections through the pyramid at, or above, the level of the IAC (figs. 3E and 3F). On CT, it courses ventromedially toward the IAC from the antrum above, medial in respect to the osseous labyrinth. The tract may extend above the IAC. More medially, the subarcuate tract arising from the mastoid antrum passes ventromedially below the arch of the superior semicircular canal (fig. 3F). It often joins the posterosuperior tract as a ventral extension that pneumatizes the petrous apex (fig. 3F). The posteromedial tract and the posterosuperior tract immediately below it (fig. 3D) are often difficult to differentiate. The cells of the posteromedial tract lie close to the vestibular aqueduct (fig. 3C). The paucity of these cells along with a narrow vestibular aqueduct have been implicated in Meniere disease, thought to be due to fibrotic labyrinthitis [22]. This cell tract may also extend far ventrally to contribute to the pneumatization of the petrous apex.

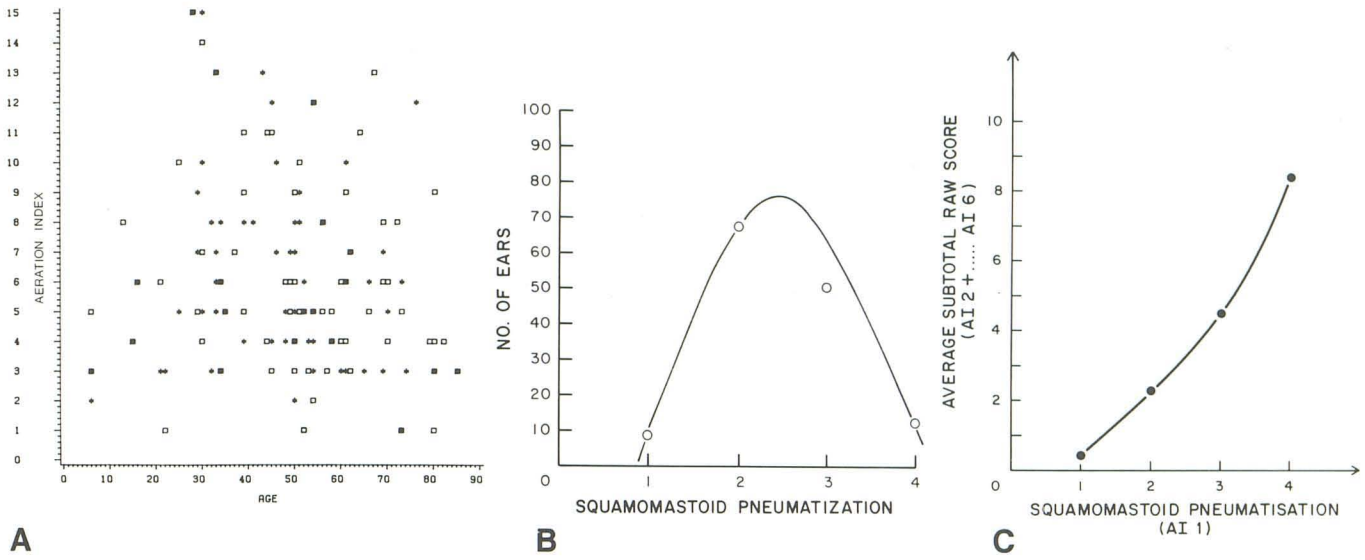

Fig. 6.—**A**, Random distribution of pneumatization and age. **B**, Plot of squamomastoid pneumatization score (abscissa) vs. total number of cases (ordinate), suggesting normal (Gaussian) distribution. **C**, Near-linear relation between squamomastoid pneumatization (abscissa) and rest of temporal bone (ordinate).

The supralabyrinthine region is pneumatized by the posterosuperior and subarcuate cell tracts (figs. 4B and 4C). The infralabyrinthine region is pneumatized by buds of pneumatization from the hypotympanum and by the posteromedial and peritubal tracts (figs. 3A, 3B, and 4C).

The petrous apex is more often partly pneumatized by tracts derived from the supra- and infralabyrinthine areas (usually the former) and from the peritubal tract (figs. 3E and 3F). The accessory regions include the squamous, the zygomaticooccipital, and the styloid. Tegmental cells may pass upward into the squamous temporal or extend into the zygomatic arch (fig. 3F). The sinal cells may extend into the occipital squama, and the tip cells into the styloid process.

Materials and Methods

We studied "normal" temporal-bone CT of 100 patients subjected to CT scans at Yale–New Haven Hospital and the Hospital of St. Raphael. In all, 141 temporal bones were analyzed. In 41 patients both ears were examined; 68 examinations were of the right ear, and 73 of the left ear. There were 52 male patients, aged 6–82 years, and 48 female patients, aged 6–85 years.

Scans were obtained on both the Pfizer 0200 and GE CT/T 8800 scanners. The majority (72 scans) were done on the GE scanner. The scanning techniques for the Pfizer have been previously described [23, 24]. Scanning technique for the GE scanner was 120 kV, 400 mA, and 9.6 sec scanning time. Prospective TARGET reconstruction was performed × 3.0–× 3.6. The images were displayed on an extended window scale of 4000 H, level 300–400. As a rule, only 0° axial scans were obtained due to limited scanning time.

All scans were initially read by at least one neuroradiologist. Criteria for a normal scan were (1) absence of bony destruction or sclerosis; (2) absence of fluid or mass in any of the temporal bone air spaces; and (3) the presence of "normal" air cells, defined by the pre-CT radiographic literature as having a sharp, well defined mucoperiosteal margin without septal thickening. The last criterion was difficult to fulfill because of the large variation in "normal" air-cell morphology on CT. Much of such morphology is difficult to demonstrate by plain radiography or conventional tomography. In view of the pathologic implications of the sclerotic squamomastoid, patients with this finding were excluded.

The degree of pneumatization in each part of the temporal bone was then analyzed by an observer after a scoring system has been devised. The following regions (aeration indices) were considered: squamomastoid, mastoid process, perilabyrinthine, petrous, peritubal, and accessory regions. The latter included squamosal, zygomatic, styloid, and occipital. The scoring system was based on a subjective evaluation of an approximate surface area of pneumatization and number of air cells on a CT slice that best demonstrated the region. A score of 1 was given to a region occupied by 10 or fewer medium-sized (2–5 mm) cells, a score of 2 given to 11–30 cells, 3 to 31–50 cells, and 4 to 51 or more. Such parametric grading was considered to be most representative of the pneumatic system. The intraobserver variability was less than 5%. An interobserver variability test was considered unnecessary, since the grading is based on relative subjective merit. Compared with plain films, a score of 1 for the squamomastoid corresponded to the "diploic" mastoid, and a score of 2–4 to the pneumatized variety.

The score of each aeration index was then tallied to give an overall raw score of pneumatization for that ear. The results were then compiled by computer.

Results

Statistical Analysis

Temporal bone pneumatization correlated poorly with age (fig. 6A) (r [squamomastoid] = −0.068; r [temporal bone total] = −0.151) and gender (r = 0.2). A plot of squamomastoid pneumatization against the number of ears suggested a normal (Gaussian) distribution, consistent with the findings of Tumarkin [25] and Diamant [26] (fig. 6B). The squamomastoid was diploic (grade 1) in nine ears and well pneumatized (grades 2–4) in the rest (table 1). Squamomastoid pneumati-

TABLE 1: **Regional Distribution of Pneumatization**

Region	No. of Ears	(%)
Squamomastoid*:		
Grade 1	9	(6.3)
Grade 2	68	(48)
Grade 3	51	(36)
Grade 4	13	(9)
Mastoid process	129	(91)
Perilabyrinthine	44	(31)
Petrous apex	50	(35)
Peritubal	38	(27)
Accessory	48	(34)

* Grade 1 = ≤10 medium-sized (2–5 mm) cells; grade 2 = 11–30 cells; grade 3 = 31–50 cells; grade 4 ≥51 cells.

TABLE 2: **Regional Symmetry of Pneumatization**

Region	Average Raw Scores*	
	Right	Left
Squamomastoid	2.52	2.44
Mastoid process	1.80	1.69
Perilabyrinthine	0.36	0.40
Petrous apex	0.49	0.59
Peritubal	0.40	0.25
Accessory	0.57	0.57
Total average	6.16	5.96

* Note that when area of temporal bone is reduced, so too is score.

zation corresponded closely to pneumatization of the mastoid process, since the latter is a downward extension of the squamomastoid. There was absence of mastoid process pneumatization in only 12 ears. These were associated with low pneumatization scores in the squamomastoid, corresponding to the poorly pneumatized mastoid type. Whereas the mastoid process is second to the squamomastoid in pneumatization, the next best pneumatized regions are the accessory (particularly the squamozygomatic [$r = 0.671$]) and the petrous apex ($r = 0.594$) (table 1). A high score in the squamomastoid is usually associated with high scores in other regions of the temporal bone (fig. 6C).

There was a high degree of symmetry in this study. The average total raw score for the right ears was 6.16 compared with 5.96 for the left ears (table 2).

Air-Cell Morphology

The size of air cells varied considerably. Cells in the periantral region were often minute and difficult to distinguish from one another in well pneumatized ears. On the other hand, poorly pneumatized ears commonly had larger, more readily distinguishable cells. Small cell clusters were more often seen immediately lateral to Körner's septum (figs. 3E and 3F). Air cells increased progressively in size from the periantral region, with the larger cells peripheral in location. Giant air cells (larger than 1.5 cm) [27] were more often seen in the petrous apex.

On CT, air cells varied in configuration and often had incomplete osseous walls. Closely abutting small cells (<2 mm) with thickened septa were difficult to distinguish from diseased cells with thickened mucosa. Focal incomplete pneumatization was often seen in the scutum, giving a "pseudotumor" appearance (fig. 7). At times this region may contain considerable unpneumatized bone, giving the appearance of an osteoma or soft-tissue mass. The pseudotumor can be distinguished from disease by its location and its tendency to merge into the walls of the air cells; also, minute air cells may be discernible within its matrix (figs. 4C and 7).

The size and configuration of the temporal bone were largely determined by the degree of pneumatization. This was particularly evident in the squamomastoid, the mastoid process, the squama, and the root of the zygoma. In fact, good pneumatization may be associated with a convex bowing of bone, suggesting that air cells were acting as an expansile mass. This was readily discernible in patients who had CT scans of both ears, so that a comparison could be made. However, it is not yet clear whether pneumatization preceded or followed bone growth.

Discussion

The following functions have been ascribed to the air cells of the ear: reception of sound, resonance, insulation, air reservoir action, acoustic dissipation [28], protection from external violence [29], and lightening of the weight of the skull [30]. The "air reservoir" function claims that during eustachian tube dysfunction, squamomastoid pneumatization provides the reserve volume of air that prevents severe negative pressure from developing in the middle ear due to mucosal air absorption [31]. Such negative pressure may predispose to tympanic membrane retraction and cholesteatoma formation.

In humans, pneumatization of the temporal bone has a normal (Gaussian) distribution [25, 26] (fig. 6B). Pneumatization is rarely markedly extensive [32–34] and is often depressed. According to Wittmaack's "environmental" theory [9, 35], otitis (e.g., serous, purulent) causes morphologic and physiologic alteration of the mucosal lining, which inhibits pneumatization. The validity of Wittmaack's work has since received support from numerous investigators [10, 25, 36–38]. The second theory, propounded by Cheatle [39, 40], takes into consideration the genetic contribution to pneumatization on the basis of research on parent-offspring, siblings, and twins [41–45]. Despite the belief that both factors are important, the relative merit of each is as yet undetermined. We have attempted to synthesize the two concepts as shown in figure 1.

The second controversial point has to do with whether the sclerotic squamomastoid is primary or secondary to otitis. Whereas the early investigators believed that the sclerotic squamomastoid represented normal development [39, 40], later authors indicated that it is due to inflammation [9, 10, 19, 36]. Sclerotic new bone has been known to develop in the postoperative ear, particularly when associated with postsurgical infection [46].

Radiography has been used extensively [14, 26, 41, 47–61] to study the development of pneumatization both in children [53–55, 58] and in adults [25, 56, 59]. Pneumatization has been reported in 14%–96% of all adults. Several authors

Fig. 7.—Axial CT of right ear. Poorly pneumatized area lateral to superior septum (*arrowheads*) above scutum, giving rise to pseudotumor (*arrow*) appearance. Small focal lucencies representing air cells can be seen in matrix.

Fig. 8.—Axial scan of patient with diploic squamomastoid. Air cell development (*arrow*) extends into predominantly diploic squamomastoid, which is less dense than cortical bone but slightly denser than unpneumatized petrous apex. The few air cells that are formed are well defined.

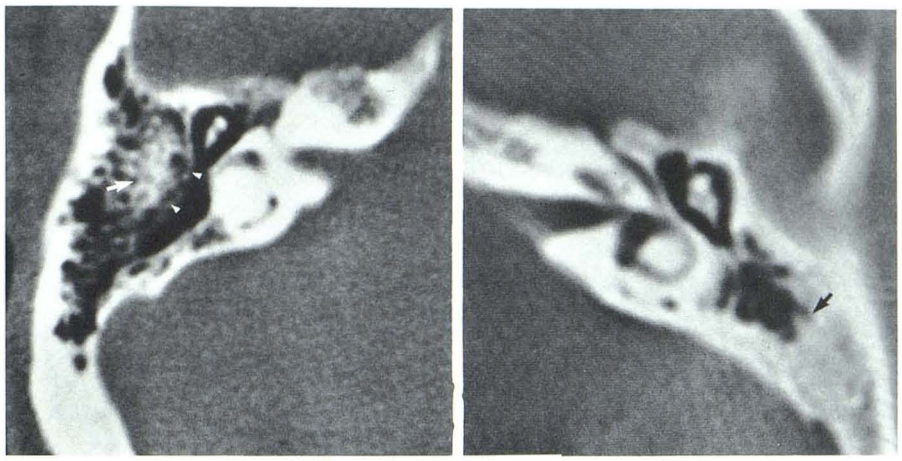

7 8

Fig. 9.—Axial scans of patient with chronic mastoiditis. Density of sclerotic bony deposition corresponds closely to density of otic capsule. Following features can be seen: much of bony deposition is in squamosal; very few to no air cells are seen; antrum is contracted (*arrow*).

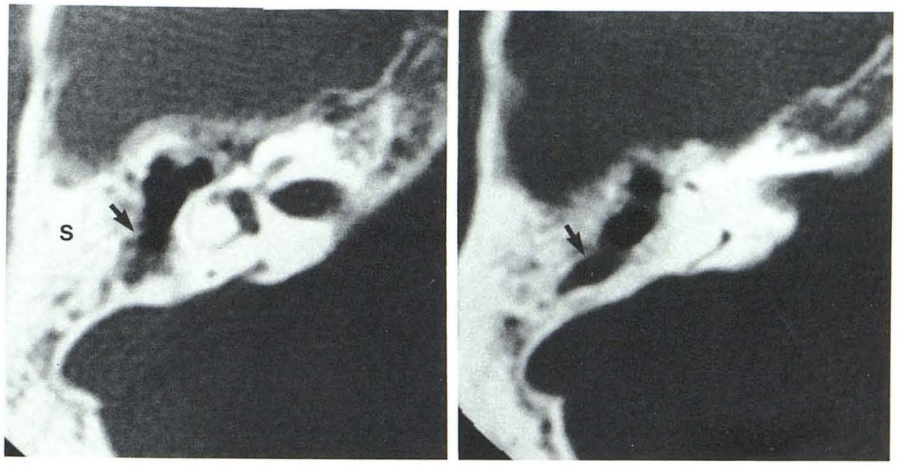

A B

have cautioned against the use of plain-film radiography [37, 52, 54, 61, 62] to assess temporal-bone pneumatization. In a study of petrositis, Fowler [57] found plain-film radiography considerably less reliable than histology for demonstrating petrous pneumatization. Even so, previously plain-film radiography offered the best method, albeit gross, of assessing pneumatization in vivo. All standard plain radiographic views have been used in the past to evaluate pneumatization [14, 16, 48, 56]. Schillinger [14, 48] used the lateral plain film for assessing air cells and attempted to establish simple radiographic norms to differentiate the poorly pneumatized from the well pneumatized ear. In the poorly pneumatized ear, air cells are confined to the periantral triangle, whereas air cells extend beyond the triangle in the well pneumatized ear (fig. 5A).

Because of the insidious nature and the intracranial complications of petrositis (Gradenigo syndrome), previous workers have emphasized the need to assess petrous-apex pneumatization [37, 52, 56, 58, 63–65], which has been found to vary from 11% to 62% [51, 52, 56, 63, 64, 66, 67]. The frequency of occurrence of petrous-apex giant air cells that, before CT, could be mistaken for an erosive lesion has been reported to be 4% [27]. Our finding of petrous-apex pneumatization in 35% of all temporal bones corresponds with the data of Schmidt [56], Hagens [67], and Glick [63]. Further, we have established that the probability of petrous-apex pneumatization corresponds directly with the degree of squamomastoid pneumatization, a view concordant with that of Kraus [52].

Symmetry of pneumatization has been found to occur in 72%–99% of the general population [37, 66]. We also found good symmetry in our series. We therefore conclude that when asymmetric pneumatization is seen on CT, the ear with the depressed system should be suspected of being diseased. The morphology of each air cell should be carefully studied for signs of new bone formation or destruction, and the surrounding bone should be assessed for sclerosis (figs. 8 and 9). In analyzing mucosal thickening, an area of incomplete pneumatization containing small air cells can be mistaken for disease (fig. 7). It is thus prudent to search for mucosal thickening in medium-sized or large air cells, preferably the latter; the previously described scutum "pseudotumor" should not be mistaken for an osteoma because of its high density. Thick sections (>1.5 mm) may also produce

spurious septal thickening by partial-volume effect.

The main advantage of CT is that it can evaluate temporal-bone pneumatization in its entirety with excellent resolution. Theoretically, the resolution of CT allows air cells as small as 2 mm to be differentiated from marrow bone, limited only by the voxel thickness. How CT compares to histology has not yet been determined.

CT identification of the course of petrosal pneumatization tracts allows presurgical prediction of spread of pus from the middle ear and mastoid, alerting the surgeon to the need for exploration into the depth of the petrous pyramid [19, 68]. Recognition of mastoid-tip pneumatization is important, because pus extending from the central tract into the tip cells may break through the bony confine of the mastoid process to present as a Bezold abscess in the neck [18].

REFERENCES

1. Anson BJ, Donaldson JA. *Surgical anatomy of the temporal bone*, 3d ed. Philadelphia: Saunders, **1981**
2. Bast TH, Anson BJ. *The temporal bone and the ear*, 1st ed. Springfield, IL: Thomas, **1949**:315–336
3. Bast TH, Forrester HB. Origin and distribution of air cells of the temporal bone. *Arch Otolaryngol* **1939**;30:183–205
4. Vasiliu DI. Contributions sur l'embryologenese de l'oreille et la pneumatisation de la mastoide et du rocher. *Int Audiol* **1968**;7:181–185
5. Williams HL. Developmental variations of the temporal bone that influence the evolution of chronic suppurative otitis media and mastoiditis and medical and surgical treatment of this syndrome. *Laryngoscope* **1969**;99:827–859
6. Shambaugh GE, Glassock ME. *Surgery of the ear*, 3d Philadelphia: Saunders, **1980**:24–25
7. McMurrich JP. *The development of the human body*. Philadelphia: P. Blakeston's Sons, **1923**:453
8. Warwick R, Williams PL. *Gray's anatomy*, 35th ed. Philadelphia: Saunders, **1973**:1142
9. Wittmaack K. Zur Frage der Bedeutung der Mittelohrentzundungen des fruhesten Kindesalters fur Spater. *Arch Ohren Nasen Kehlkopfh* **1931**;129:207–250
10. Palva T, Palva A. Size of the human mastoid air cell system. *Acta Otolaryngol* (Stockh) **1966**;62:237–251
11. Ojala L. Contributing to the physiology and pathology of mastoid air cell formation. *Acta Otolaryngol [Suppl]* (Stockh) **1950**;86:1–134
12. Ojala L. Pneumatization of the bone and environmental factors: experimental studies in chick humerus. *Acta Otolaryngol [Suppl]* (Stockh) **1957**;133:1–28
13. Beaumont GD. The effects of exclusion of air from pneumatized bones. *J Laryngol Otol* **1966**;80:236–249
14. Schillinger R. Pneumatization of the mastoid. *Radiology* **1939**;33:54–67
15. Shapiro R. *Radiology of the normal skull.* Chicago: Year Book Medical, **1981**:326–340
16. Lindsay JR. Petrous pyramid of temporal bone: pneumatization and roentgenologic appearance. *Arch Otolaryngol* **1940**;31:231–235
17. Allam AF. Pneumatization of the temporal bone. *Ann Otol Rhinol Laryngol* **1969**;78:48–64
18. Tremble GE. Pneumatization of the temporal bone. *Arch Otolaryngol* **1934**;19:172–182
19. Shuknecht HF. *Pathology of the ear.* Cambridge, MA: Harvard University Press, **1974**:79–85
20. Meltzer PE. The mastoid cells: their arrangement in relation to the sigmoid portion of the transverse sinus. *Arch Otolaryngol* **1934**;19:326–335
21. Virapongse C, Sarwar M, Bhimani S, Sasaki C, Shapiro R. Computed tomography of temporal bone pneumatization. II: Petrosquamosal suture and septum. *AJNR* **1985**;6:561–568
22. Hall SF, O'Connor AF, Thakkar CH, Wylie IG, Morrison AW. Significance of tomography in Meniere's disease: periaqueductal pneumatization. *Laryngoscope* **1983**;93:1551–1553
23. Virapongse C, Rothman SLG, Kier EL, Sarwar M. Computed tomographic anatomy of the temporal bone. *AJR* **1982**;139:739–749
24. Virapongse C, Rothman SLG, Sasaki C, Kier EL. The role of high resolution computed tomography in evaluating disease of the middle ear. *J Comput Assist Tomogr* **1982**;6:711–720
25. Tumarkin A. On the nature and significance of hypocellularity of the mastoid. *J Laryngol Otol* **1959**;73:34–44
26. Diamant M. Otitis and size of the air cell system. *Acta Radiol* (Stockh) **1940**;21:543–548
27. Dubois PJ, Roub LW. Giant air cells of the petrous apex: tomographic features. *Radiology* **1978**;129:103–109
28. Tumarkin A. On the nature and vicissitudes of the accessory air spaces of the middle ear. *J Laryngol Otol* **1957**;71:65–99
29. Eagleton WP. A new classification of bones forming the skull. *Trans Am Acad Ophthalmol Otol* **1935**;21–58
30. Proetz AW. Observation upon the formation and function of the accessory nasal sinus and the mastoid cells. *Ann Otol Rhinol* **1922**;31:1083–1100
31. Jackler RK, Schindler RA. Role of the mastoid in tympanic membrane reconstruction. *Laryngoscope* **1984**;94:495–500
32. Lo WWM, Zapanta E. Pneumatization of the occipital bone as a cause of radiolucent skull lesions. *AJNR* **1983**;4:1249–1250
33. Madeira JT, Summers GW. Epidural mastoid pneumatocele. *Radiology* **1977**;122:727–728
34. Parks RE. Unilateral mastoid hypertrophy *AJNR* **1982**;3:196–197
35. Wittmaack K. The significance of middle ear inflammation of infancy (abstracted by Keen JA). *J Laryngol Otol* **1931**;46:782–784
36. Gans H, Wlodyka J. Mastoid pneumatization in chronic otitis media. *Arch Otolaryngol* **1966**;83:343–346
37. Diamant M. Otitis and pneumatization of the mastoid bone. *Acta Otolaryngol [Suppl]* (Stockh) **1940**;41:1–149
38. Schulter-Ellis FP. Population differences in cellularity of the mastoid process. *Acta Otolaryngol* (Stockh) **1979**;87:461–465
39. Cheatle AH. The infantile types of the temporal bone and their surgical importance. *Lancet* **1910**;1:491–493
40. Cheatle AH. The etiology and prevention of chronic middle ear suppuration. *Acta Otolaryngol* (Stockh) **1923**;5:283–294
41. Dahlberg G, Diamant M. Hereditary character of the cellular system in the mastoid process. *Arch Otolaryngol* **1945**;33:378–389
42. Boes LR, Younger LI. Abnormal pneumatization of temporal bone. *Ann Otol Rhinol Laryngol* **1956**;61:836–849
43. Albrecht W. Zur Frage der Pneumatisation des Mittelohres: histolische Untersuchungen im Schlafenbein des Neugeborenen. *Acta Otolaryngol* (Stockh) **1930**;14:221–228
44. Schwartz M. Untersuchungen zur individullen Histologie des Bindengewebes. *Arch Ohren Nasen Kehlkopfh* **1931**;129:1–29
45. Dillon IG, Gourevitch IB. Research on the pneumatization of the nasal accessory sinuses and of the mastoid processes and on the shape of the sell turcica in twins. *AJR* **1936**;35:782–785
46. Ojala K, Lahti R, Palva A, Sorri M. Postoperative roentgenological findings and changes after mastoid obliteration. *J Laryngol Otol* **1983**;97:393–398

47. Schwartz M. Die Bedeutung der hereditaren Anlage fur die Pneumatization der Warzenfortsatze und der Nasennebenhohlen. *Arch Ohren Nasen Kehlkopfh* **1929**;123:161–232
48. Schillinger R. Roentgenologic aspects of mastoiditis. *AJR* **1938**;39:193–201
49. Lindsay JR. Suppuration in the petrous pyramid. *Ann Otol Rhinol Laryngol* **1938**;47:3–34
50. Lindsay JR. Chemotherapy in the treatment of complications of acute middle ear suppuration. *Ann Otol Rhinol Laryngol* **1941**;50:159–178
51. Lindsay JR. Pneumatization of the petrous pyramid. *Ann Otol Rhinol Laryngol* **1941**;50:1109–1113
52. Kraus L. Die Pyramidenspitzen-pneumatisation im Roentgenbild. *Arch Ohren Nasen Kehlkopfh* **1931**;128:307–338
53. Kawamura S, Okabe K, Mogi S, Terao A. The normal development of the mastoid pneumatic cells. *J Otorhinol Soc Jpn* **1963**;66:909–912
54. Rubensohn G. Mastoid pneumatization in children at various ages. *Acta Otolaryngol* (Stockh) **1965**;60:11–14
55. Evans WA. The value of the roentgen study of mastoid disease in children under five. *AJR* **1923**;10:382–385
56. Schmidt G. Uber die Pyramidenspitizenpneumatization. *Z Hals Nasen Ohrenheilkunde* **1937**;2:93–108
57. Fowler EP. The correlation of x-ray and pathologic findings in suppuration of the petrous pyramid. *Trans Am Otol Soc* **1935**;25:215–228
58. Jackson CCR. Morphologic and roentgenologic aspects of the temporal bone: study of 536 bones with special references to pneumatization. *Arch Otolaryngol* **1938**;28:561–580
59. Turner AL, Porter WG. The structural type of the mastoid process, based upon the skiagraphic examination of one thousand crania of various races of mankind. *J Laryngol Otol* **1922**;37:161–175
60. Oku T, Hasegawa M, Watanabe I. Meniere's disease and mastoid pneumatization. *Acta Otolaryngol* (Stockh) **1980**;89:118–120
61. Jones MF. Symposium on certain fundamentals in regard to suppuration of the petrous pyramid. *Anat Arch Otol* **1935**;22:515–516
62. Anson BJ, Wilson JG, Gaardsmoe JP. Air cells of petrous portion of temporal bone in a child four and a half years old. *Arch Otolaryngol* **1938**;27:588–605.
63. Glick HN. Microscopic observations of the petrous apex. *Ann Otol Rhinol Laryngol* **1933**;42:175–185
64. Belinoff F, Balan M. Uber den Bau der Pyramidspitze. *Monatsschr Ohrenheilk* **1930**;64:1185–1188
65. Gradenigo G. Uber die Paralyse des Nervous abducens bei Otitis. *Arch Ohrenheilk* **1907**;74:149–187
66. Myerson MC, Rubin H, Gilbert JG. Anatomic studies of the petrous portion of the temporal bone. *Arch Otolaryngol* **1934**;20:193–210
67. Hagens EW. Anatomy and pathology of the petrous bone based on a study of 50 temporal bones. *Arch Otolaryngol* **1934**;19:556–573
68. Williams HL. Latent or dormant disease in the pneumatic cell tracts of the temporal bone. *Trans Am Acad Ophthalmol Otol* **1966**;70:545–558